Engineering Geology 264 (2020) 105413

Contents lists available at ScienceDirect

Engineering Geology

journal homepage: www.elsevier.com/locate/enggeo

Characteristics of in-situ stress distribution in Zhengzhuang Region, Southern Qinshui Basin, China and its stress path during depletion

Peng Zhang[a,d], Zhaoping Meng[a,b,*], Shu Jiang[c,d], Xiaoming Chen[a]

[a] College of Geosciences and Surveying Engineering, China University of Mining and Technology (Beijing), Beijing 100083, PR China
[b] State Key Laboratory of Coal and CBM Co-mining, Shanxi Jincheng Anthracite Mining Group Company, Ltd., Jincheng, Shanxi 048000, PR China
[c] Key Laboratory of Tectonics and Petroleum Resource of the Ministry of Education, Faculty of Earth Resources, China University of Geosciences, Wuhan 430074, PR China
[d] Energy and Geoscience Institute, University of Utah, UT 84108, USA

ARTICLE INFO

Keywords:
In-situ stress
Coalbed methane
Depletion
Reservoir stability
Qinshui Basin

ABSTRACT

The in-situ stress and its behavior during depletion are critical for investigation of the reservoir permeability, wellbore stability, enhanced oil recovery (e.g. stimulation), fault reactivation, and reservoir management. However, the rules that govern in situ stress variation in coalbed methane (CBM) reservoirs and its influences on reservoir stability are still unclear due to the matrix shrinkage effect. In this study, the distribution characteristics of in-situ stress in the Zhengzhuang (ZZ) region were investigated by multi-loop hydraulic fracturing tests and a theoretical stress-depletion response model was built to reveal the dynamic rules of in-situ stress during CBM depletion. Additionally, considering the redistribution of in-situ stress and the limitation induced by fault friction coefficient, a criterion for stress-based failure was developed to analyze the stability of CBM reservoir. The results suggest that in the ZZ block, the fracturing pressure, closure pressure, and the maximum and minimum horizontal principal pressures are positively correlated with burial depth. During drainage, the horizontal principal stress reduces and the effective horizontal principal stress increases linearly as pore pressure reduction. During gas desorption phase, the horizontal principal stress decreases and the effective horizontal principal stress increases non-linearly under weak desorption, whereas both decline non-linearly in response to strong desorption. In addition, the failure criterion for CBM reservoirs indicates that reservoirs in a normal faulting stress regime are the most easily damaged, which may occur during drainage or desorption. However, reservoir damage can only be induced under strong desorption in a strike-slip faulting stress regime and cannot occur in a reverse faulting stress regime. If faults do develop in reservoirs, the reservoir stability is governed by the fault friction coefficient. Finally, by combining the data, the changes in in-situ stress and the stability of the reservoirs during depletion in the ZZ region were revealed and its implications for CBM development were discussed.

1. Introduction

Coalbed methane (CBM) has become a practical and reliable substitute for conventional natural gas which is in short supplies worldwide (Meng et al., 2011; Xie et al., 2019). China has 36.81 $\times$ 10^{12} m^3 CBM resources at depths of < 2000 m, ranking third in the word (Meng et al., 2011; Li et al., 2017). Thus, CBM has become an important supply source of natural gas in China. However, in order to extract CBM efficiently, some critical engineering issues need to be solved (Chen et al., 2018a; Ju et al., 2018; Lau et al., 2017; Durucan and Edwards, 1986). In-situ stress is one of the key parameters that influence the development of CBM at most of the coal basins in China, the United States, Australia, and Canada (Li et al., 2019; Zhao et al., 2019; Ju et al., 2018; Rajabi et al., 2017; Chen et al., 2018a, 2018b).

In-situ stress refers to the internal stress that is present in the Earth's crust and can be divided into self-weight and tectonic stress (Bell, 1996; Kang et al., 2010). Self-weight stress is caused by an overburden, such as an overlying rock mass, and can usually be calculated by the weight of the mass. However, the mechanisms that lead to tectonic stress are relatively complicated, and it is difficult to precisely describe tectonic stress (Kang et al., 2010). The accurate measurement of in-situ stress is essential for the estimation of well productivity, as in situ stress has a direct influence on the aperture and orientation of the permeable fractures. A key difference between conventional reservoirs and coal reservoirs is the dual porosity medium observed in coal. Most pores within the coal matrix are too narrow to provide effective paths for the seepage of gas. That is, the permeability of coal seams is mainly governed by fractures (Paul and Chatterjee, 2011; Laubach et al., 1998).

* Corresponding author at: College of Geosciences and Surveying Engineering, China University of Mining and Technology (Beijing), Beijing 100083, PR China.
E-mail address: mzp@cumtb.edu.cn (Z. Meng).

https://doi.org/10.1016/j.enggeo.2019.105413
Received 26 February 2019; Received in revised form 4 November 2019; Accepted 11 November 2019
Available online 15 November 2019
0013-7952/ © 2019 Elsevier B.V. All rights reserved.

Thus, non-uniform in-situ stress can significantly affect the permeability of the coal (Enever and Henning, 1997; Pan and Connell, 2012). For example, the coal permeability in a normal faulting stress regime is higher than that in a strike-slip faulting stress regime (Meng et al., 2011; Li et al., 2019), which is due to the fact that there is a relatively low compressive stress around normal faults. Increased in-situ stress narrows the fractures, resulting in a decline in the permeability of the coal. It is widely accepted that coal permeability reduces exponentially with an increase in effective stress (McKee et al., 1988; Ju et al., 2018). In-situ stress also has a significant influence on the stability of a wellbore, the amount of oil recovered (e.g. stimulation), and reservoir management (Rajabi et al., 2017; Bell, 1996; Zoback et al., 2003; Liu et al., 2016). Therefore, an accurate estimation of in-situ stress state can effectively guide the CBM exploration and production.

In-situ stress does not remain constant during depletion, which challenges traditional understanding (Kim and Hosseini, 2017). The variation in pore pressure caused by reservoir depletion or injection of fluid into a reservoir will change the in-situ stress of the reservoir (Mortazavi and Atapour, 2018). Researches have been carried out on the formation of conventional reservoirs (Goulty, 2003; Hillis, 2000; Segall and Fitzgerald, 1998; Mortazavi and Atapour, 2018; Kim and Hosseini, 2017), which has indicated that the reservoir horizontal stress decreases significantly as pore pressure declines during fluid extraction (Hillis, 2000; Goulty, 2003) and the rate of change in the horizontal stress per unit pore pressure depends on the reservoir lithology (Hillis, 2000; Goulty, 2003). It is also apparent that changes in the in-situ stress have a great impact on the physical properties of reservoirs, and can therefore induce serious engineering issues (e.g. sand production, borehole instability during drilling, casing collapse, and fault reactivation) (Hillis, 2000; Goulty, 2003). Thus, accurate prediction of the in-situ stress of a reservoir during depletion is of great significance for accurate characterization of an oil or gas reservoir, and is of considerable concern for development and completion, enhanced oil recovery projects, and reservoir management. However, unlike conventional oil or gas reservoirs, CBM reservoirs exhibit unique characteristics during depletion because matrix shrinkage results in additional volumetric strain(Shi and Durucan, 2005; Levine, 1996; Liu and Harpalani, 2014). The in-situ stress variation mechanism in a CBM reservoir is obviously different from that in conventional oil/gas reservoirs. However, minimal study has so far been carried out concerning CBM development (Liu and Harpalani, 2014; Fan and Liu, 2018; Feng et al., 2018; Saurabh and Harpalani, 2018). The changes rules of the in-situ stress associated with drainage and gas desorption and their influences on reservoir stability, permeability and strength are still unclear. In addition, in-situ stress (before or during depletion) is always affected by the geological structure, particularly faults (Zoback, 2010). The strength of the fault friction in the Earth's crust limits the magnitude of in-situ stress. The frictional force in the fault planes cannot overcome the shear stress that occurs during depletion, and the reservoirs slip along the fault plane, causing the production of coal fines and a drop in permeability (Townend and Zoback, 2000). Thus, knowledge concerning the limitations that fault friction strength has on in-situ stress will benefit the optimization of CBM production.

The study area of Zhengzhuang (ZZ) region is located in the southern Qinshui basin, which is the China's largest CBM exploitation base. In this work, the distribution characteristics of in-situ stress in ZZ region were investigated by multi-loop hydraulic fracturing tests. And theoretical models were built to describe the dynamical rules of in-situ stress during CBM depletion. Additionally, taking into account of the redistribution of in-situ stress and the limitation of fault friction coefficient (μ_i), a stress-based failure criterion was developed to analyze the coal reservoir stability during depletion. Finally, combining the actual data, the change rules of in-situ stress and reservoir stability during depletion in ZZ region were revealed and its implication for CBM development was discussed.

2. Geological background

Qinshui Basin is situated in the southeast of the Shanxi Province, China, and is known for its abundant coal and CBM resources (Fig. 1A) (Chen et al., 2018a). It is a large synclinorium (bilateral symmetry) with the axial striking NNE-SSW and is surrounded by the Taihang mountains in the east, Huo mountains in the west, Wutai mountains to the north, and Zhongtiao mountains in the south (Fig. 1B) (Cai et al., 2011; Wang et al., 2012). The study area (ZZ region) is located in the south of the Qinshui Basin, which has become one of the most favorable regions for CBM development (Fig. 1B). Many faults and folds were developed in this region with axials striking NE-NEE (Huang et al., 2019). The Houchengyao and Sitou faults, the main faults in the study area, have significant effects on the in-situ stress. The coal seams have been deformed by four periods of tectonic movement, namely, Indosinian (the Late Permian-Late Triassic), Yanshan (the Middle Jurassic to Cretaceous), Early Himalayan (Late Eocene) and Late Himalayan (Late Neogene) period after coal forming (Wang et al., 2012). In the Indosinian period, as the North China Craton collided with the South China Plate in the south and the Siberian Plate in the north, the region was subjected to an intense compressional stress field striking N-S (Wang et al., 2012). However, this apparently had only a weak effect on the CBM reservoir. In the Yanshan period, the tectonic activity was dominated by NW-SE compression stress due to the NW subduction of the Kula-Pacific plates, which was recorded as a series of NE/NNE trending folds and NW/EW joints. The strong tectonic and magmatic activities were beneficial to the generation of CBM and reservoir cleats (Wang et al., 2012). However, the lithosphere thinned because of the continuing subduction of the Pacific plate and its collision with the Indian plate. The regional stress was then reversed to NW-SE extensional stress during the Early Himalayan period (Wang et al., 2012). Some NNE normal faults and joints were generated. During the late Himalayan period the mantle activity weakened, which led to the regional stress changing to NE-SW compressive stress, which resulted in several NW trending secondary folds. As the Qinshui Basin is near the large-scale strike-slip fault, multi-period slip movements including compressional strike slips and extensional strike slips also occurred in this area, which had a significant effect on the distribution and enrichment of the CBM (Wang et al., 2016). The current regional stress field was drawn as per the World Stress Map Database, which suggests that the orientation of the regional stress is NE dominated. The maximum horizontal stress ranges from 0.3 to 38 MPa and the minimum stress ranges from 0.1 to 23.3 MPa. The regional stress state is mainly a strike-slip regime (Fig. 1A).

The coal in the basin was mainly formed during the Pennsylvanian and the Permian, during which the strata were generally deposited in a transitional marine / non-marine environment, including the Benxi, Taiyuan, Shanxi, Xiashihezi, Shangshihezi, and Shiqianfeng formations (Fig. 1D). Coal seam No. 3 of the Shanxi formation and coal seam No. 15 of the Taiyuan formation are the two main CBM reservoirs (Lv et al., 2012). The burial depth of these two coal seams ranges primarily between 350 and 1300 m with the thickness ranging from 2 to 7 m (Fig. 1C). Due to strong metamorphism, the coal is anthracite with a maximum vitrinite reflectance ($R_{o,\ max}$) of 2.89–4.34% and the gas content is also high, ranging from 10 to 37 m^3/t (Huang et al., 2019). The physical and mechanical properties of the coal from the roof and floor of the reservoir are different. The Young's modulus, Poisson's ratio, compressive strength, and tensile strength of these two coal seams range from 0.21 to 2.08 GPa, 0.27 to 0.33, 2.51 to 25.31 MPa, and 0.09 to 1.15 MPa, respectively (Meng et al., 2012).

3. Methodology

Because of the low permeability of CBM reservoirs, technology such the multi-loop hydraulic fracturing test has become a common and effective method to measure the in-situ stress of wells (Chen et al., 2018a;

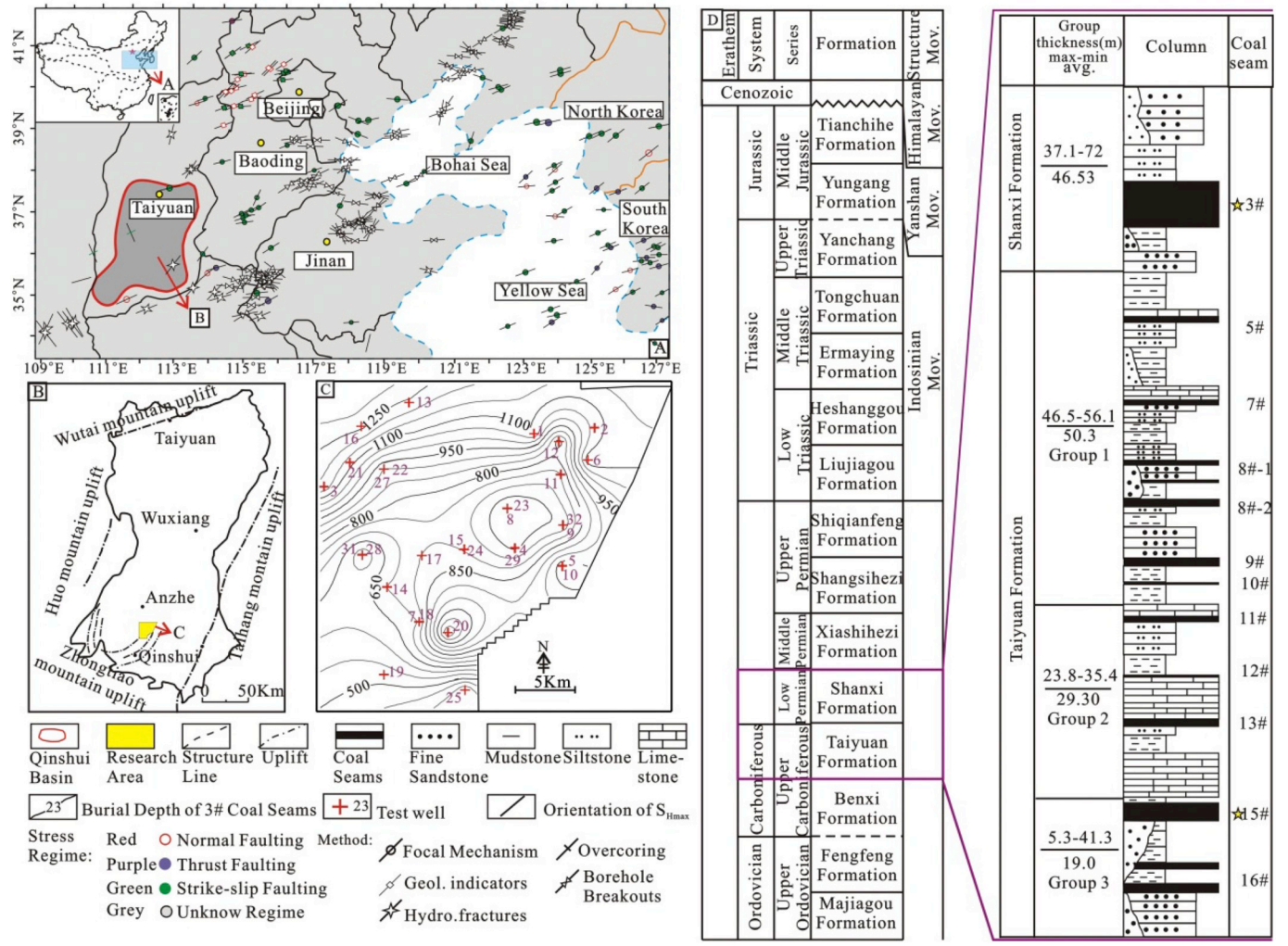

Fig. 1. (A)The regional stress field from World Stress Map Database (Heidbach et al., 2016) and the Location of the Qinshui Basin in China; (B) Location of the study area in Qinshui Basin; (C) The buried depth of No.3 coal seams and the distribution of testing wells; (D) Stratigraphic column of study area.

Haimson and Cornet, 2003). The test system mainly consists of five parts (including pump injection equipment, electric pressure gauge, packer, pipelines and tubing strings, and well-shut equipment) and assembled as shown in (Fig. 2A). In this work, 31 test wells have been conducted in No.3 and No. 15 coal seams of ZZ region.

The multi-loop hydraulic fracturing test was performed in each well according to China Earthquake industry standard DB/T 14–2000. Before testing, the equipment was assembled as Fig. 2A and the connection of this test system was checked to ensure the injection liquid didn't leak. In the testing process, water was injected into the wellbore with a relatively high injection rate, which makes the bottom hole pressure increase rapidly. When the bottom hole pressure was higher than the fracturing pressure, the coal seam was broken and created new fractures which extended along the maximum horizontal principal stress orientation (Fig. 2C). As the injection water leak rapidly, the bottom hole pressure dropped greatly. Then, the testing well was shut-in and the critical pressure was recorded as fracturing pressure (P_f). In this test process, to obtain a high quality in-situ data, four test cycles were conducted in each well and the bottom hole pressure data was collected every second. Finally, based on these data, the curve of bottom hole pressure and time could be drawn, as shown in (Fig. 2B).

In order to obtain a further key parameter with which to describe a reservoir (closing pressure, P_c), two or three test cycles with good fracturing and closing effects were selected from the four test cycles, and the in-situ pressure fall data from the shut-in stage of these were analyzed using the time square root method and plotted in a time square root plot, where the ordinate and the abscissa are the pressure and the square root of the time, respectively. The plot is given in Fig. 3, in which the closure pressure is the point that deviates from the line (Haimson and Cornet, 2003; Zoback et al., 2003; Liu et al., 2016). Generally, the closure pressure is an indicative of the minimum principal stress. Furthermore, based on the test results, it is apparent that the vertical stress is always greater than the closure pressure. The minimum principal stress is therefore equal to the minimum horizontal principal stress (σ_h) (Eq. (1)):

$$\sigma_h = P_c \tag{1}$$

Assumed the coal seam is homogeneous and isotropic and non-fluid permeable, and obey linear elastic theory. The effective hoop stress ($\sigma_{\theta\theta}$) at the wellbore wall can be described by Eq. (2) (Zoback, 2010). The minimum effective hoop stress occurs at the point ($\theta = 0°$), where the hydraulic fracture can be easily induced. When the minimum effective hoop stress is equal to $-T_0$ (T_0: the coal/rock tensile strength), the coal/rock will be fractured. Then, the fluid pressure in the well bottom (P_{wb}) is equal to the fracturing pressure (P_f) and the maximum horizontal principal stress (σ_H) can be expressed as Eq. (3) (Zoback, 2010; Hubbert and Willis, 1957):

$$\sigma_{\theta\theta} = \sigma_H + \sigma_h - 2(\sigma_H - \sigma_h)\cos\theta - P_o - P_{wb} - \sigma^{\Delta T} \tag{2}$$

$$\sigma_H = 3\sigma_h - P_f - P_o + T_0 - \sigma^{\Delta T} \tag{3}$$

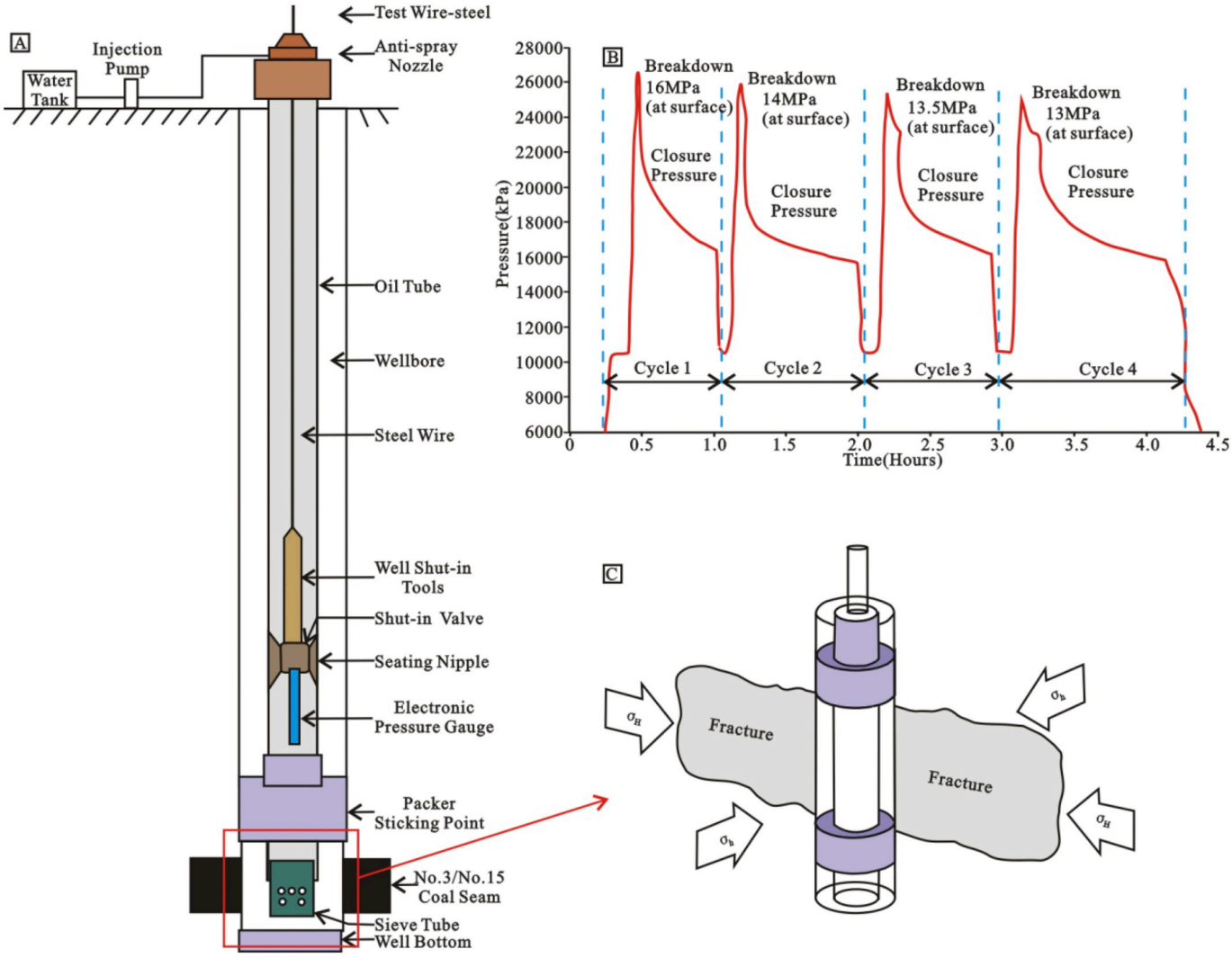

Fig. 2. (A) Schematic diagram of the multi-loop hydraulic fracturing test; (B) In-situ stress measurement curves of well 10; (C) Schematic of fracture propagation.

where $\sigma^{\Delta T}$ is thermal stress, which is small and can be ignored, MPa; P_o is the reservoir pressure, MPa; and T_0 is the coal/rock tensile strength, MPa; θ is measured from the azimuth of σ_H; P_{wb} is the fluid pressure in the well bottom. Note that if the test cycle, chosen to analyze in-situ stress, is not the first cycle, in other words, the well has been fractured by first cycle, the coal tensile strength is equal to zero ($T_0 = 0$). As the buried depth of the coal reservoir is shallow, the stress caused by temperature difference usually can be ignored. Then, the Eq. (3) can be simplified as follow:

$$\sigma_H = 3\sigma_h - P_f - P_o \quad (4)$$

The vertical principal stress (σ_v) is induced by the overlying rock weight, thus vertical principal stress can be estimated by the bulk density of the overlying formation. A toal of 116 in-situ stress test results around the word were counted by Hoek and Brown (1980), which provide the following prediction formula of σ_v:

$$\sigma_v = 0.027D \quad (5)$$

where D is the burial depth from the surface in meters.

4. Results

The results of the multi-loop hydraulic fracturing tests for the 31 wells in the ZZ region are plotted in Fig. 4, which suggest that the coal seam is buried at 351.3–1268.8 m, with an average of 842.40 m. The fracturing pressure ranges from 6.66 to 31.38 MPa (mean: 18.18 MPa) with a pressure gradient ranging from 1.48 to 2.96 MPa/100 m (mean: 2.21 MPa/100 m). The closure pressure range is 6.24–29.09 MPa (mean: 16.90 MPa/100 m) with the pressure gradient ranging from 1.34 to 2.85 MPa/100 m (mean: 2.05 MPa/100 m). The magnitudes of σ_H, σ_h, and σ_v were calculated using Eqs. (1), (4), and (5), respectively, which indicate that σ_H is between 10.48 and 44.57 MPa with an average of 25.26 MPa, σ_h varies from 6.24 to 29.09 MPa with an average of 16.90 MPa, and σ_v ranges from 9.49 to 34.26 MPa, with an average of 22.75 MPa (Fig. 4). Overall, it appears that all of the main CBM regions in China have similar in-situ stress magnitudes (Chen et al., 2018a, 2018b; Ju et al., 2018; Meng et al., 2011; Shen et al., 2018; Zhao et al., 2019). However, the in-situ stress in the study area is higher than that observed in other CBM regions of the world, such as the American Black Warrior (σ_h, 1–6 MPa), the Australian Sydney and Bowen Basins (σ_h, 1–10 MPa) (McKee et al., 1988; Enever and Henning, 1997). The study found that 62.5% of the σ_h is between 10 and 18 MPa and 34.4% of the σ_h ranges from 18 to 30 MPa, which suggests the ZZ region is subjected to strong to moderate stress, according to the standards used for judgment (0–10 MPa, weak; 10–18 MPa, moderate; 18–30 MPa, strong; and > 30 MPa, super-strong) (Kang et al., 2009).

By analyzing the P_f, P_c, σ_H, and σ_h, we can obtain the relevant relationships between these parameters and the burial depth by regression analysis, as shown in Fig. 5. The results indicate that the P_f, P_c, σ_H, and σ_h increase linearly with the burial depth, governed by the

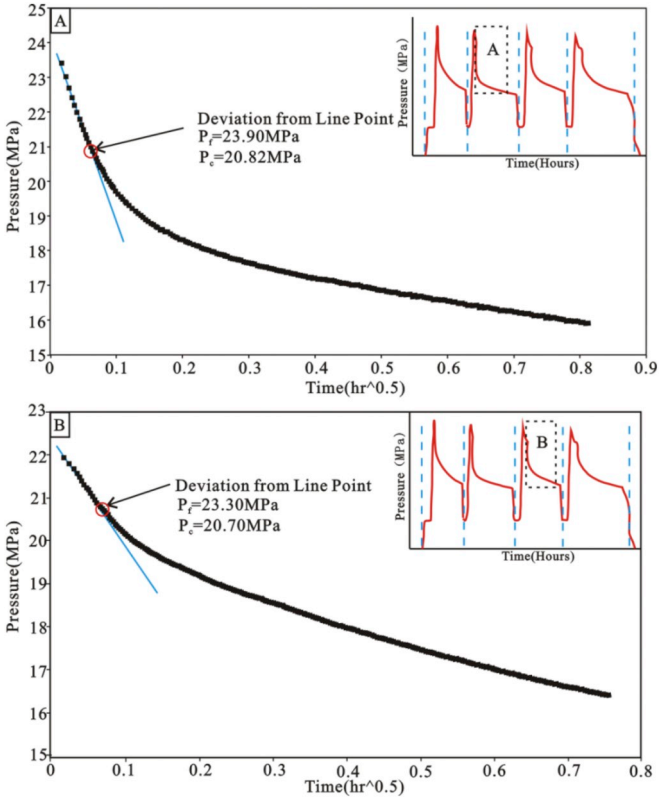

Fig. 3. Calculated curves for shut-in pressure of circle 2 and circle 3 for well 10.

following formulas:

$$P_f = 0.0190D + 2.2935\ (R^2 = 0.6482) \quad (6)$$

$$P_c = 0.0170D + 2.4531\ (R^2 = 0.5937) \quad (7)$$

$$\sigma_H = 0.0238D + 5.2512\ (R^2 = 0.4337) \quad (8)$$

$$\sigma_h = 0.0171D + 2.4536\ (R^2 = 0.5937) \quad (9)$$

The relevant relationships between the fracturing pressure and closure pressure are also derived, demonstrating that fracturing pressure increases linearly with the growth in closure pressure (Fig. 6). The closure pressure can therefore be obtained from the fracturing pressure on the basis of the following relationship:

$$P_c = 0.9288P_f - 0.0757\ (R^2 = 0.9672) \quad (10)$$

The minimum horizontal principal stress is a key parameter in the development of a CBM, acting as a primary control on the fracture pressure gradient, hydraulic fracture propagation, and well stability. Based on the measured P_o, σ_v and σ_h, the relationship between effective vertical and minimum horizontal stresses in the CBM reservoirs can be obtained, as shown in Eq. (11). However, the correlation between the effective minimum horizontal principal stress and effective vertical principal stress is poor (Fig. 7). This may be caused by tectonic stress (plate movement, magmatic activity, fault, etc.).

$$\sigma_h - P_o = 0.671(\sigma_v - P_o) \quad (11)$$

This relationship indicates that the CBM reservoir has an effective stress coefficient similar to other sedimentary rocks in oil and gas basin (Hubbert and Willis, 1957; Matthews and Kelly, 1967; Zoback and Healy, 1984). For instance, the empirical effective stress coefficient (k) equation was proposed by Matthews and Kelly (1967) to predict the pore pressure at which circulation is lost. When the hydraulic fracture propagates away from the wellbore, this pore pressure is essentially equivalent to the minimum principle stress (σ_{min}) (Zoback, 2010). Thus, they proposed the equation ($\sigma_{min} - P_o = k(\sigma_v - P_o)$; $k = \frac{\sigma_{min} - P_o}{\sigma_v - P_o}$) to predict minimum principle stress. Based on the test result, the minimum principle stress in this study area is the minimum horizontal principal stress. Then, the following relationship can be obtained, as shown in Eq. (12). The ration of effective stress (k) in this study area can also be estimated ($k \approx 0.671$), which is much lower than that of shales in deep petroleum basins (commonly $k \approx 0.8$) (Meng et al., 2011; Zhang et al., 2017).

$$\sigma_h - P_o = k(\sigma_v - P_o) \quad (12)$$

where, k is the effective stress ratio, $k = \frac{\sigma_h - P_o}{\sigma_v - P_o}$.

Based on the relative magnitudes of the three principal stress and the stress field classification (Anderson, 1951), two main types of stress regimes can be identified in the study area; a normal faulting stress regime ($\sigma_v > \sigma_H > \sigma_h$) and strike-slip faulting stress regime ($\sigma_H > \sigma_v > \sigma_h$). This is in accordance with the regional stress, which is thought to be caused by the same mechanism within the area studied. The stress in the region may be caused by the subduction of the Pacific plate and the collision of the Indian plate. Furthermore, the measured in-situ stress indicates that the three principal stresses (σ_H, σ_h, and σ_v) are unstable. The normal faulting stress regime is distributed at a depth of 637.82 to 1188.05 m. The relationship between stress (σ_H, σ_h) and depth can be expressed by Eqs. (13) and (14). However, the strike-slip faulting stress regime is distributed widely, ranging between depths of 351.3 and 1268.8 m. We obtained the relationship between stress (σ_H, σ_h) and depth using Eqs. (15) and (16).

Normal faulting stress regime:

$$\sigma_H = 0.027D - 2.7044 \quad (13)$$

$$\sigma_h = 0.016D + 0.4175 \quad (14)$$

Strike-slip faulting stress regime:

$$\sigma_H = 0.040D - 3.8578 \quad (15)$$

$$\sigma_h = 0.0241D - 2.1976 \quad (16)$$

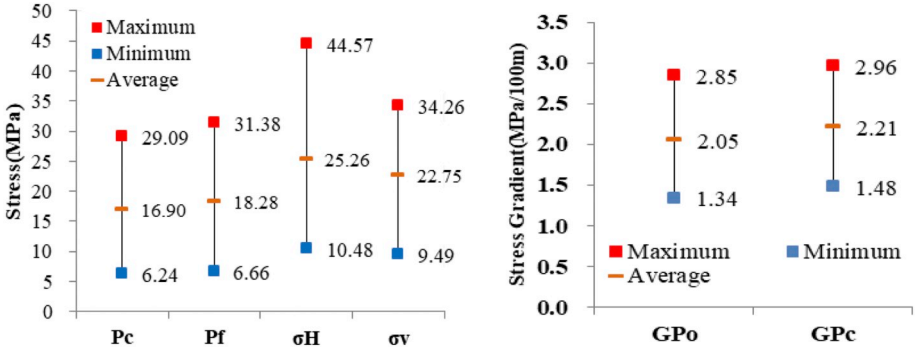

Fig. 4. Stock chart of multi-loop hydraulic fracturing test parameters in ZZ region.

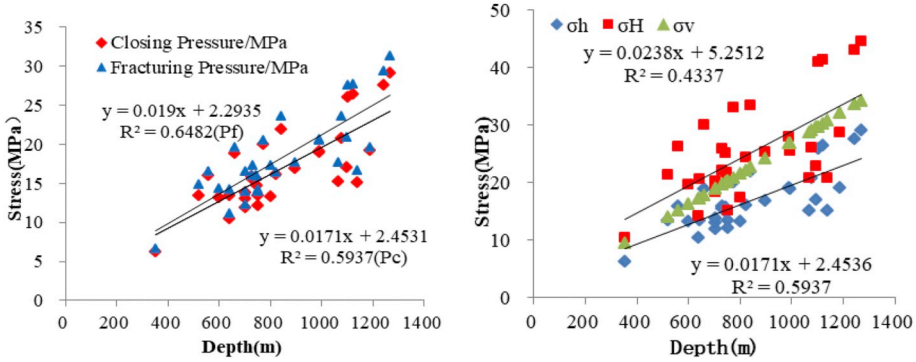

Fig. 5. (A) Relationships between closing pressure vs. buried depth, and fracturing pressure vs. buried depth; (B) Relationship between σ_H, σ_h and σ_V vs. buried depth in ZZ blcok.

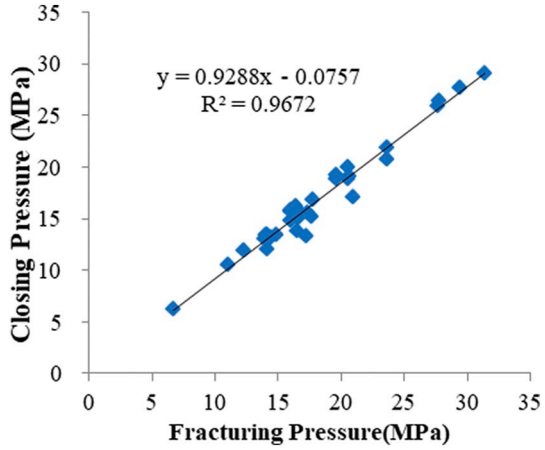

Fig. 6. Relationships between closing pressure and fracturing pressure in ZZ region.

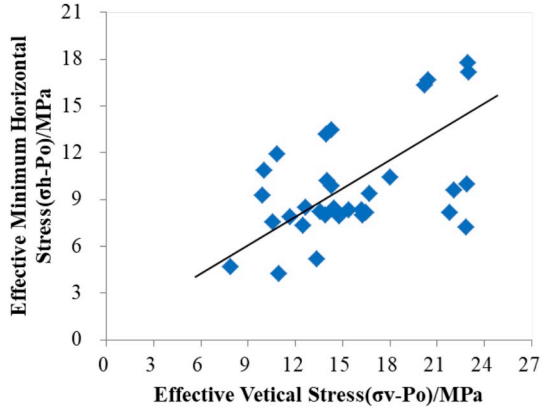

Fig. 7. Relationship of the effective vertical principle stress and the effective minimum horizontal principle stress in ZZ region.

5. Discussions

5.1. Theoretical models describing the stress-depletion response in CBM development

The variation in pore pressure during reservoir production and fluid injection into a reservoir alters the state of stress of the reservoir and the surrounding rocks, which leads to several problems such as fault reactivation, borehole instability, and sand production among others, but which can also lead to some positive results, such as improvements in permeability (Mortazavi and Atapour, 2018; Saurabh and Harpalani, 2018; Feng et al., 2018; Liu and Harpalani, 2013; Fan and Liu, 2018). In order to replicate in-situ stress, three commonly used experimental models (including the constant volume model, the uniaxial strain model and the hydrostatic stress model) have been previously suggested, among which the uniaxial strain model was the most widely accepted for reservoir engineering (Liu and Harpalani, 2014; Hubbert and Willis, 1957). The coal bed is thin (of just a few meters), but extends to approximately a few kilometers in the lateral direction. The ratio of the lateral extent to the thickness is > 10:1. Thus, the uniaxial strain model also can be applied to study the dynamic rules for the in-situ stress in CBM reservoirs with some accuracy (Fig. 9) (Segall and Fitzgerald, 1998). Unlike the development of conventional reservoirs, there are two phases in the development of CMB: drainage and desorption. In this study, the CBM reservoir is assumed as linearly elastic and isotropic, with horizontal extensions. Based on the linear elasticity theory, the relationship between the horizontal strain increment ($\Delta\varepsilon_h$) and the effective stress increments (ΔS_h, ΔS_H and ΔS_v) during the process of drainage can be expressed as: (Goulty, 2003):

$$\Delta\varepsilon_h = \frac{1}{E}[\Delta S_h - \upsilon(\Delta S_H + \Delta S_v)] + \frac{1}{3k_s}\Delta P \tag{17}$$

$$S_h = \sigma_h - P \tag{18}$$

where ΔP is the change in pore pressure, MPa; σ_h is the horizontal principle stress, MPa; E is Young's modulus of coal frame; υ is the Poisson's ratio of coal frame; and k_s is the bulk modulus of the coal grains.

Under uniaxial strain conditions (in Fig. 9), which is widely accepted in reservoir engineering, the vertical stress remains constant due to an unchanged overburden and the lateral strain is fixed and maintained at zero during depletion. Then, the following equation can be obtained:

$$\begin{cases} \Delta\varepsilon_h = \Delta\varepsilon_H = 0 \\ \Delta\sigma_v = 0;\ \Delta S_h = \Delta S_H \\ \Delta S_v = -\Delta P \end{cases} \tag{19}$$

As $E = 3k(1 - 2\upsilon)$, where k is the frame bulk modulus, so by integrating Eqs. (17)–(19), the ratio of ΔS_h to ΔP can be given as follows:

$$\frac{\Delta S_h}{\Delta P} = \frac{\alpha(1 - 2\upsilon) - (1 - \upsilon)}{(1 - \upsilon)} \tag{20}$$

where α is the Biot's coefficient and is defined by $\alpha = 1 - k/k_s$.

Thus, the ratio of $\Delta\sigma_h$ to ΔP can be expressed as:

$$\frac{\Delta\sigma_h}{\Delta P} = \frac{\alpha(1 - 2\upsilon)}{(1 - \upsilon)} \tag{21}$$

If the rock is of poor cementation and contains many factures, α is approximately equal to 1 (Zhao et al., 2003). A significant number of cleats and pores are distributed within coal seams, and therefore $\alpha \approx 1$ for CBM reservoirs. However, in the process of desorption, the adsorbed

gas released from the coal matrix results in shrinkage of the matrix and additional volumetric strain, which in turn leads to a very different stress response (Levine, 1996; Fan and Liu, 2018). In this study, the model describing the response to stress-depletion in the desorption phase was derived based on the following constitutive equation, which is the stress-strain relationship for a homogenous, isotropic, thermo-elastic, and porous medium and was first proposed by Nowacki (1975) and Bear and Corapcioglu (1981):

$$\Delta S_{ij} = 2G\Delta\varepsilon_{ij} + \lambda\Delta\varepsilon_v\delta_{ij} + \left(\lambda + \frac{2}{3}G\right)\alpha_T\Delta T\delta_{ij} \tag{22}$$

where ΔS_{ij} is the change in effective stress, G is shear modulus ($G = \frac{E}{2(1+\upsilon)}$), λ is Lamé's first parameter ($\lambda = \frac{\upsilon E}{(1+\upsilon)(1-2\upsilon)}$), $\Delta\varepsilon_{ij}$ is the incremental values of linear strain, $\Delta\varepsilon_v$ is the change in volumetric strain($\Delta\varepsilon_v = \Delta\varepsilon_{xx} + \Delta\varepsilon_{yy} + \Delta\varepsilon_{zz}$), δ_{ij} is the Kronecker delta, α_T is the coefficient of volumetric thermal expansion and ΔT is the change in temperature.

Similar to the Palmer & Mansoori model and Shi & Durucan model, the relationship between thermal contraction and matrix shrinkage was deduced using the Langmuir isotherm model, which is expressed as follows (Shi and Durucan, 2004; Palmer and Mansoori, 1998):

$$\alpha_T\Delta T = \Delta\varepsilon_s \tag{23}$$

where $\Delta\varepsilon_s$ is the change in the sorption-induced volumetric strain due to the variation of temperature.

Recently, many kinds of empirical approaches have been adopted to quantitatively model sorption-induced volumetric strain. One such model was proposed by Levine (1996), which is given as:

$$\Delta\varepsilon_s = \varepsilon_L\left(\frac{P}{P_L + P} - \frac{P_0}{P_L + P_0}\right) \tag{24}$$

where P_0 is initial pore pressure, MPa; ε_L is the maximum volumetric strain, P_L is the pressure where coal attain 50% of the maximum strain, MPa.

The magnitude of Young's Modulus is not constant during depletion. The research conducted by Dave (2017) indicated that E decreases continuously with the desorption of methane, which can be expressed as:

$$E = a\ln P + c \tag{25}$$

Where a and c are constant, which are determined by coal physical property.

By substituting Eqs. (23)–(25) into Eq. (22), the stress-strain relationships for the three principal stresses are expressed as: `

$$\begin{cases} \Delta S_{xx} = \dfrac{a\ln P + c}{(1+\upsilon)}\Delta\varepsilon_{xx} + \dfrac{\upsilon(a\ln P + c)}{(1+\upsilon)(1-2\upsilon)}\Delta\varepsilon_v + \dfrac{a\ln P + c}{3(1-2\upsilon)}\Delta\varepsilon_s \\ \Delta S_{yy} = \dfrac{a\ln P + c}{(1+\upsilon)}\Delta\varepsilon_{yy} + \dfrac{\upsilon(a\ln P + c)}{(1+\upsilon)(1-2\upsilon)}\Delta\varepsilon_v + \dfrac{a\ln P + c}{3(1-2\upsilon)}\Delta\varepsilon_s \\ \Delta S_{zz} = \dfrac{a\ln P + c}{(1+\upsilon)}\Delta\varepsilon_{zz} + \dfrac{\upsilon(a\ln P + c)}{(1+\upsilon)(1-2\upsilon)}\Delta\varepsilon_v + \dfrac{a\ln P + c}{3(1-2\upsilon)}\Delta\varepsilon_s \end{cases} \tag{26}$$

Recalling the uniaxial strain condition (Eq. (19)), the relationship between the effective horizontal principal stress and the pore pressure in the desorption phase can be expressed as follows:

$$\begin{aligned} \Delta S_h = \Delta S_H = \Delta S_{xx} = \Delta S_{yy} \\ = \frac{-\upsilon}{1-\upsilon}(P - P_0) + \frac{a\ln P + c}{3(1-\upsilon)}\varepsilon_L\left(\frac{P}{P_L + P} - \frac{P_0}{P_L + P_0}\right) \end{aligned} \tag{27}$$

Also, the relationship between the horizontal principal stresses in the desorption phase can be expressed as follows:

$$\Delta\sigma_h = \Delta\sigma_H = \frac{1-2\upsilon}{1-\upsilon}(P - P_0) + \frac{a\ln P + c}{3(1-\upsilon)}\varepsilon_L\left(\frac{P}{P_L + P} - \frac{P_0}{P_L + P_0}\right) \tag{28}$$

Finally, the dynamic models describing the change in the effective horizontal principal stress and horizontal principal stress during CBM depletion can be summarized as:

$$\begin{aligned} f_\sigma(P) = \Delta\sigma_h = \Delta\sigma_H \\ = \begin{cases} \dfrac{1-2\upsilon}{1-\upsilon}(P - P_0), & P > P_d \\ \dfrac{1-2\upsilon}{1-\upsilon}(P - P_0) + \dfrac{a\ln P + c}{3(1-\upsilon)}\varepsilon_L\left(\dfrac{P}{P_L + P} - \dfrac{P_d}{P_L + P_d}\right), & P \le P_d \end{cases} \end{aligned} \tag{29}$$

$$\begin{aligned} f_S(P) = \Delta S_h = \Delta S_H \\ = \begin{cases} \dfrac{-\upsilon}{1-\upsilon}(P - P_0), & P > P_d \\ \dfrac{-\upsilon}{1-\upsilon}(P - P_0) + \dfrac{a\ln P + c}{3(1-\upsilon)}\varepsilon_L\left(\dfrac{P}{P_L + P} - \dfrac{P_d}{P_L + P_d}\right), & P \le P_d \end{cases} \end{aligned} \tag{30}$$

Where $f_\sigma(P)$ is the change in horizontal principal stresses due to the variation of pore pressure; $f_S(P)$ is the change in effective horizontal principal stresses induced by the variation of pore pressure, and P_d is critical desorption pressure, MPa.

Based on (29) and (30), dynamic rules describing the three principal stresses during CBM depletion are plotted in Fig. 10. These plots suggest that the dynamic evolution of in-situ stresses with pressure drawdown is a complex process.

During the process of drainage ($P > P_d$): there is no gas desorbed from the coal matrix. Based on (29) and (30), the horizontal principal stresses are reduced linearly with the decline in pore pressure (at the rate of $\frac{1-2\upsilon}{1-\upsilon}$), but the rate of reduction is less than that of the pore pressure ($\left(\frac{\Delta\sigma_{H/h}}{\Delta P}\right)_{Drainage} < 1$) (Fig. 10A: point a to b). The effective horizontal principal stresses increase linearly (at the rate of $\frac{-\upsilon}{1-\upsilon}$) with a rate that is also lower than that of pore pressure ($-1 < \left(\frac{\Delta S_{H/h}}{\Delta P}\right)_{Drainage} < 0$) (Fig. 10B: point a to b).

During the process of desorption ($P \le P_d$): the dynamic evolution of the in-situ stresses is a more complex process. Based on the magnitude of the stress induced by desorption, the mechanisms by which the in-situ stress changes can be divided into two; the low desorption effect and the strong desorption effect:

1) Low desorption effect: the horizontal principal stresses decrease non-linearly with the drop in pore pressure, and the decreasing rate of horizontal principal stresses in this phase is higher than that in the drainage phase but lower than that of the pore pressure ($1 > \left(\frac{\Delta\sigma_{H/h}}{\Delta P}\right)^{Low}_{Desorption} > \left(\frac{\Delta\sigma_{H/h}}{\Delta P}\right)_{Drainage}$)(Eq.(29)) (Fig. 10A: point b to d). In contrast, the effective horizontal principal stresses increase non-linearly and the increasing rate is lower than that in the drainage phase ($\left(\frac{\Delta S_{H/h}}{\Delta P}\right)_{Drainage} < \left(\frac{\Delta S_{H/h}}{\Delta P}\right)^{Low}_{Desorption} < 0$) (Eq.(30)) (Fig. 10B: point b to d).

2) Strong desorption effect: although a non-linear decline in the horizontal principal stresses can also be observed, the decline rate of the horizontal principal stresses is greater than that of the pore pressure ($\left(\frac{\Delta\sigma_{H/h}}{\Delta P}\right)^{High}_{Desorption} > 1$) (Eq.(29)) (Fig. 10A: point b to c). There is an obvious change in the effective horizontal principal stresses, which decreases non-linearly with the depletion ($0 < \left(\frac{\Delta S_{H/h}}{\Delta P}\right)^{High}_{Desorption}$) (Eq.(30)) (Fig. 10B: point b to c).

In addition, under the conditions of uniaxial strain, the vertical stress is constant and equal to the weight of the overlying formations during the whole process of depletion, so the increments of the effective vertical stress are equal to the decrements of the pore pressure ($\Delta\sigma_V = 0$; $\frac{\Delta S_V}{\Delta P} = -1$).

Summarizing the above analysis, the following relationships can be used to describe the evolution of in-situ stress due to depletion:

$$\begin{cases} 0 < \left(\frac{\Delta\sigma_{H/h}}{\Delta P}\right)_{Drainage} < \left(\frac{\Delta\sigma_{H/h}}{\Delta P}\right)_{Desorption}^{Low} < 1 < \left(\frac{\Delta\sigma_{H/h}}{\Delta P}\right)_{Desorption}^{High} \\ -1 < \left(\frac{\Delta S_{H/h}}{\Delta P}\right)_{Drainage} < \left(\frac{\Delta S_{H/h}}{\Delta P}\right)_{Desorption}^{Low} < 0 < \left(\frac{\Delta S_{H/h}}{\Delta P}\right)_{Desorption}^{High} \end{cases} \quad (31)$$

$$\begin{cases} \Delta\sigma_v = 0 \\ \Delta S_v = -\Delta P \end{cases} \quad (32)$$

5.2. Failure criterion of CBM reservoirs during depletion

Based on the traditional theories, in-situ stresses are assumed to be constant and no damage occurs in reservoirs during depletion (Fig. 11). However, as suggested by the discussion in the above section, the in-situ stress changes dynamically in response to changes in the pore pressure. The redistribution of in-situ stress has a significant influence on reservoir stability (Mortazavi and Atapour, 2018). The criteria for the failure of CBM reservoirs during depletion under two geological conditions are discussed in the following section, including intact CBM reservoirs and faulted CBM reservoirs.

5.2.1. Failure criterion of intact CBM reservoirs during depletion

As a brittle rock, coal should obey the Mohr-Coulomb criterion; this can therefore be applied to evaluate the stability of a coal seam during depletion. A series of Mohr's diagrams was drawn to describe the changes in stress, as shown in Fig. 12. If a coal bed is destroyed and a failure plane caused by depletion, the influence of the middle principal stress was ignored, the normal and shear stress on the failure face can be evaluated with the following equations:

$$\sigma_n = 0.5(S_1 + S_2) + 0.5(S_1 - S_2)\cos 2\beta \quad (33)$$

$$\tau = 0.5(S_1 - S_3)\sin 2\beta \quad (34)$$

Where, τ is the shear stress, MPa; σ_n is the effective normal stress, MPa; β is the angle between the normal direction of the failure plane and the maximum principal stress. S_1 and S_3 are the effective maximum principal stress and the effective minimum principal stress respectively, MPa.

A linearized Mohr–Coulomb failure envelope is usually referred to as Mohr–Coulomb failure, which can be written as (Zoback, 2010):

$$\tau = \mathbb{C} + \sigma_n \tan\varphi \quad (35)$$

Where $\mathbb{C}$ is the cohesive strength, MPa; $\mu = \tan\varphi$ is the coefficient of internal friction.

As cohesion strength ($\mathbb{C}$) can't be measured accurately, it is commonly replaced by unconfined compressive strength (C_0). The relationship between them is (Zoback, 2010):

$$C_0 = 2\mathbb{C}[\sqrt{\mu^2+1} + \mu] \quad (36)$$

Substituting Eqs. (33), (34) and (36) into Eq. (35), the following equation can be given as follows:

$$S_1 = C_0 + [\sqrt{\mu^2+1} + \mu]^2 S_3 \quad (37)$$

Substituting $S_1 = \sigma_1 - P$ and $S_3 = \sigma_3 - P$ in Eq. (37), the linearized form of the Mohr failure criterion of in-situ stresses can be given as:

$$\sigma_1 = C_0 + [\sqrt{\mu^2+1} + \mu]^2\sigma_3 + (1 - [\sqrt{\mu^2+1} + \mu]^2)P \quad (38)$$

Generally, there are three types of in-situ states. Assuming that the initial magnitudes of the three principal stresses are σ_{H0}, σ_{h0}, and σ_{V0}, respectively. The stress-based failure criterion is therefore as follows (Fig. 12).

(1) When $\sigma_{V0} > \sigma_{H0} > \sigma_{h0}$, the Mohr failure criterion during depletion can be written as:

$$\sigma_{V0} = C_0 + [\sqrt{\mu^2+1} + \mu]^2(\sigma_{h0} + f_\sigma(P)) + (1 - [\sqrt{\mu^2+1} + \mu]^2)P \quad (39)$$

In the drainage process, the decrement in pore pressure is equal to the increment in effective vertical stress ($\Delta S_V = -\Delta P$) and higher than the increment in effective minimum horizontal principal stress ($\Delta S_h < -\Delta P$). This means that the Mohr circle expands to the right and approaches the Mohr–Coulomb failure envelope. Entering the desorption phase, the increments of the effective vertical stresses ($\Delta S_V{}^1$) are the same as that of the drainage ($\Delta S_V{}^1 = \Delta S_V = -\Delta P$), but the increment of effective minimum horizontal principal stress ($\Delta S_h{}^1$) is lower than that of the drainage for low desorption coal ($\Delta S_h{}^1 < \Delta S_h < -\Delta P$). Moreover, if the coal has a strong desorption effect, the effective minimum horizontal principal stress will decrease ($\Delta S_h{}^1 < 0$) (Fig. 12C). Both of these principles indicate that gas desorption can lead to a rapid movement of the Mohr circle to the failure envelope and accelerating the failure of the reservoir.

(2) When $\sigma_{H0} > \sigma_{V0} > \sigma_{h0}$, the Mohr failure criterion during depletion can be written as

$$\sigma_{H0} + f_\sigma(P) = C_0 + [\sqrt{\mu^2+1} + \mu]^2(\sigma_{h0} + f_\sigma(P)) + (1 - [\sqrt{\mu^2+1} + \mu]^2)P \quad (40)$$

During drainage, the increment in effective minimum principal stress is equal to the increment in maximum principal stress due to the decrease in pore pressure, but the increment rates of both stresses are lower than that of in pore pressure ($\Delta S_h = \Delta S_H < -\Delta P$), which suggests that the Mohr circle will have a constant radius and will move away from the failure envelope. However, the increment of the effective horizontal principal stress ($\Delta S_h{}^1$ and $\Delta S_H{}^1$) is lower in the process of gas desorption than in the drainage ($\Delta S_h{}^1 = \Delta S_H{}^1 < \Delta S_h = \Delta S_H < -\Delta P$), meaning that the Mohr circle moves at a reduced rate. However, if the coal has a stronger desorption effect, the Mohr circle would move towards the left, and could induce reservoir failure ($\Delta S_h{}^1 = \Delta S_H{}^1 < 0$). Over the whole depletion process, the radius of the Mohr circle remains constant.

(3) When $\sigma_{H0} > \sigma_{h0} > \sigma_{V0}$, the Mohr failure criterion during depletion can be written as:

$$\sigma_{H0} + f_\sigma(P) = C_0 + [\sqrt{\mu^2+1} + \mu]^2\sigma_{V0} + (1 - [\sqrt{\mu^2+1} + \mu]^2) \quad (41)$$

As seen illustrated in Fig. 12, in the depletion process, the Mohr circle would shrink leftward and move away from the failure envelope, which means that the failure is not caused by drainage and gas desorption. But there also are some differences. During drainage, the increment in effective vertical stress is greater than the effective maximum horizontal principal stress, resulting in a reduction in the radius of the Mohr circle ($\Delta S_H < -\Delta P = \Delta S_V$). For low desorption coal, the increment in effective maximum horizontal principal stress is lower than that of the drainage ($\Delta S_H{}^1 < \Delta S_H$) (Fig. 12H). If the desorption effect is strong, the effective maximum horizontal principal stress will decline ($\Delta S_H{}^1 < 0$).

Based on the above analyses, it can be summarized that CBM reservoir failure can be induced by both drainage and gas desorption. However, there are significant differences in the failure criteria for different in-situ states and sorption effects. A reservoir in a normal faulting stress regime ($\sigma_{V0} > \sigma_{H0} > \sigma_{h0}$) can be damaged most easily; damage can occur in both the drainage and gas desorption phases. However, the effects of drainage and low gas desorption cannot cause reservoir failure in a strike-slip faulting stress regime ($\sigma_{H0} > \sigma_{V0} > \sigma_{h0}$); damage can only take place during the period of strong gas desorption. Significantly, if the reservoir is subjected to reverse faulting stress regimes ($\sigma_{H0} > \sigma_{h0} > \sigma_{V0}$), the dynamic changes in the in-situ stress will tend to retain the stability of a reservoir; in other words the reservoir cannot be destroyed during depletion.

5.2.2. Failure criterion of faulted CBM reservoirs during depletion

The CBM reservoir usually contains widely distributed faults,

fractures, and other planar discontinuities at many different scales, which are induced by endogenic and exogenic geological processes (Zhang et al., 2017). The magnitudes of the regional stresses are usually limited by the frictional strength of these planar discontinuities. Leonardo da Vinci conducted the first systematic study of friction, after which Guillaume Amontons carried out significant research in this area and elucidated the law of friction, also known as Amontons' Law. He found that frictional sliding will be induced in faults when the ratio of shear to normal stress exceeds the friction coefficient (Zoback, 2010).

$$\frac{\tau}{\sigma_n} = \mu_i \tag{42}$$

Where μ_i is the friction coefficient, dimensionless.

The friction coefficient is a material property of faults, which is determined by its surface roughness, normal stress level, rock type and fault gouge. Under a high normal stress ($\sigma_n \geq$ 10MPa), the friction coefficient of fault plane varies in a narrow range from 0.6 to 1and is irrelevant to surface roughness, normal stress and sliding velocity, commonly known as Byerlee's law (Byerlee, 1978).

The normal stress and shear stress acting on a fault plane can be evaluated by Eqs. (33) and (34). There is an optimal slipping angle (β) in faults, where the faults prior to other faults tend to slip under the stress. This equation can be calculated as follows (Zoback, 2010):

$$\beta = \frac{\pi}{4} + \frac{1}{2}\tan^{-1}\mu_i \tag{43}$$

Substituting the Eqs. (33), (34) and (43) into (42), the relationship among the S_1, S_3 and μ_i for faulted reservoirs can be obtained.

$$\frac{S_1}{S_3} = \frac{\sigma_1 - P}{\sigma_3 - P} = [\sqrt{\mu_i^2 + 1} + \mu_i]^2 \tag{44}$$

Eq. (44) indicates that if the ratio of S_1 to S_3 exceeds the value of $[\sqrt{\mu_i^2 + 1} + \mu_i]^2$, slipping will occur. Therefore, the following criterion for failure in faulted CBM reservoirs during depletion can be acquired:

$$\begin{cases} \dfrac{\sigma_{V0} - P}{\sigma_{h0} + f_\sigma(P) - P} \leq [\sqrt{\mu_i^2 + 1} + \mu_i]^2, (\sigma_{V0} > \sigma_{H0} > \sigma_{h0}) \\ \dfrac{\sigma_{H0} + f_\sigma(P) - P}{\sigma_{h0} + f_\sigma(P) - P} \leq [\sqrt{\mu_i^2 + 1} + \mu_i]^2, (\sigma_{H0} > \sigma_{V0} > \sigma_{h0}) \\ \dfrac{\sigma_{H0} + f_\sigma(P) - P}{\sigma_{V0} - P} \leq [\sqrt{\mu_i^2 + 1} + \mu_i]^2, (\sigma_{H0} > \sigma_{h0} > \sigma_{V0}) \end{cases} \tag{45}$$

5.3. Implications for the CBM development in ZZ region

5.3.1. Change rules of in-situ stress in ZZ region

The physical and mechanical properties of the two coal seams were also investigated (Table 1), demonstrating that the Young's modulus and Poisson's ration range from 0.21 to 2.08 GPa (mean: 1.09 GPa) and from 0.27 to 0.33 (mean: 0.31), respectively (Meng et al., 2012). In this study, Young's modulus is assumed to be constant during the depletion of CBM. The maximum volumetric strain (ε_L) of no. 3 and no. 5 coal seams in the southern Qinshui basin were obtained by Meng (2018) as 1.381%. Thus, the dynamic changes in the horizontal principal stresses and the effective horizontal principal stresses during depletion in the ZZ region can be theoretically calculated as follows:

$$f_\sigma(P) = \Delta\sigma_{xx} = \Delta\sigma_{yy} = \begin{cases} 0.5507(P - P_0), P < P_d \\ 0.5507(P - P_0) + 7.267\left(\dfrac{P}{P_L + P} - \dfrac{P_d}{P_L + P_d}\right), P \geq P_d \end{cases} \tag{46}$$

$$f_S(P) = \Delta S_{xx} = \Delta S_{yy} = \begin{cases} -0.4492(P - P_0), P < P_d \\ -0.4492(P - P_0) + 7.267\left(\dfrac{P}{P_L + P} - \dfrac{P_d}{P_L + P_d}\right), P \geq P_d \end{cases} \tag{47}$$

Significant differences were observed in the initial pore pressure (P_0), the Langmuir pressure (P_L) where coal attains 50% of the maximum strain, the critical desorption pressure (P_d), and the gas content ($G_{s,Vdaf}$)for each of the wells in the ZZ region, as seen in Table 2. These parameters were entered into Eqs. (46) and (47), from which the mechanisms for the changes in the minimum horizontal principal stress (σ_h) and the effective minimum horizontal principal stress (S_h) during depletion in each of the wells of the ZZ region can be revealed, as plotted in Figs. 13 and 14.

The results indicate that σ_h reduces linearly during the drainage process (at a speed of 0.5507 MPa per 1 MPa of pore pressure) and that S_h increases linearly (at a speed of 0.4493 MPa per 1 MPa of pore pressure). This is associated with the reduction in the permeability of the CBM reservoir. However, when entering desorption, σ_h decreases non-linearly. Meanwhile, except for wells 3, 5, 13, and 21, there is an obvious change in S_h, which decreases non-linearly rather than increases with the drop in pore pressure due to the strong desorption. During this phase, the rates of decrease in σ_h and S_h rise with the increasing desorption, which improves the permeability. The S_h near wells 3, 5, 13, and 21 all increases gently during the initial phase of gas desorption. The desorption effect is enhanced with the decline in pore pressure, and the S_h near these wells will decline rapidly as in the other wells do.

Table 1
Basic physical parameters in ZZ region.

Parameters	Values (Min-Max) Ave.	References
Compressive strength (Saturation) /C_0	8.14(MPa)	this paper
Friction coefficient/μ	0.6	Zoback (2010)
Internal friction coefficient/μ_i	0.7	Feng et al. (2011)
Young's modulus/E	(0.21–2.08)1.09 (GPa)	Meng et al. (2012)
Posson's ration/υ	(0.27–0.33)0.31	Meng et al. (2012)
Maximum volumetric strain /ε_L	0.0138	Meng (2018)

Table 2
Basic parameters of each wells in ZZ region and critical value of pore pressure for the CBM reservoir stability.

Wells	Po/MPa	$G_{s,Vdaf}$/(m^3/t)	P_L/MPa	V_L/(m^3/t)	P_d/Mpa	P_{cv}/MPa	Stress states
3	9.21	28.34	2.95	36.35	10.44	1.10	Normal
4	6.27	25.81	3.04	41.44	5.02	2.57	fault
5	10.60	1.51	3.43	37.07	0.15	\	regime
6	7.94	13.93	2.95	40.44	1.55	0.92	
7	5.36	23.40	2.89	41.82	3.67	0.28	
8	6.47	10.86	2.48	42.60	0.85	\	
10	12.63	1.39	3.48	46.01	0.11	\	
13	10.53	22.25	2.81	32.44	6.14	\	
14	3.59	22.29	2.18	31.80	5.11	\	Strike-
15	6.59	26.98	2.09	36.58	5.87	\	slip fault
16	11.32	15.97	3.33	34.40	2.89	\	regime
17	5.53	23.42	2.18	37.74	3.57	\	
18	5.07	22.40	2.57	36.27	4.15	\	
19	4.19	20.61	2.00	31.36	3.83	\	
20	9.34	21.54	2.79	38.53	3.54	\	
21	10.08	11.44	2.21	35.29	1.06	\	
22	7.51	10.00	2.99	44.90	0.86	\	
23	5.64	8.70	2.69	36.66	0.84		
26	8.75	28.23	2.93	44.43	5.11	\	
27	8.74	16.59	2.54	40.74	1.74	\	
28	5.63	19.30	2.75	38.66	2.74	\	
29	7.06	20.75	2.57	35.36	3.65	\	

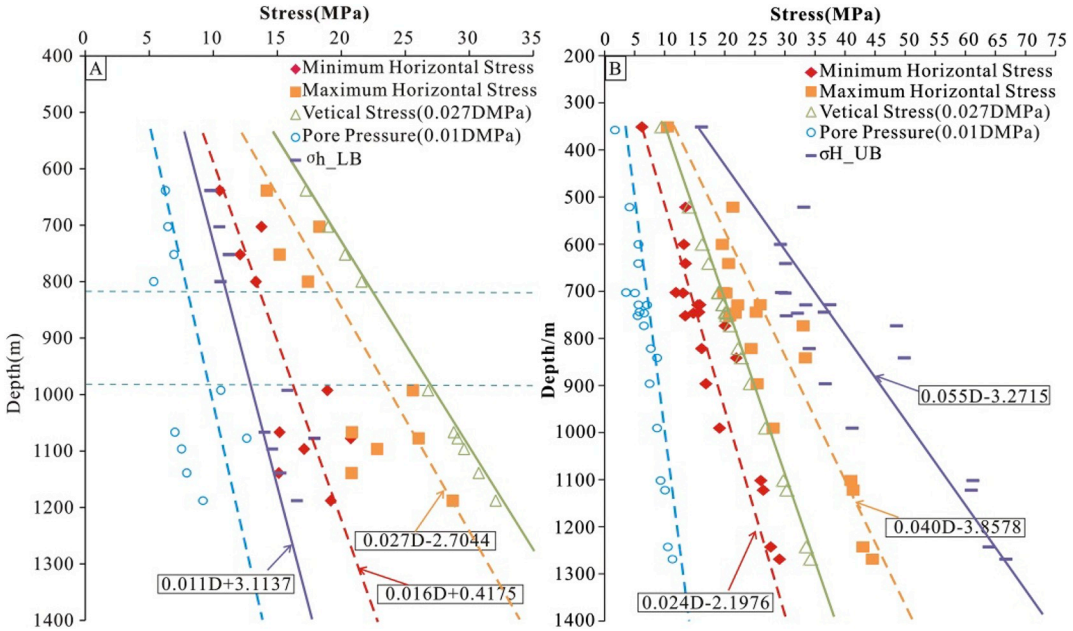

Fig. 8. The relationship between stresses/pressure (including P_o, σ_H σ_h and σ_v) and buried depth, and the limit value of σ_h and σ_H limited by fault friction strength in ZZ region; A - normal faulting stress regime, B - Strike-slip faulting stress.

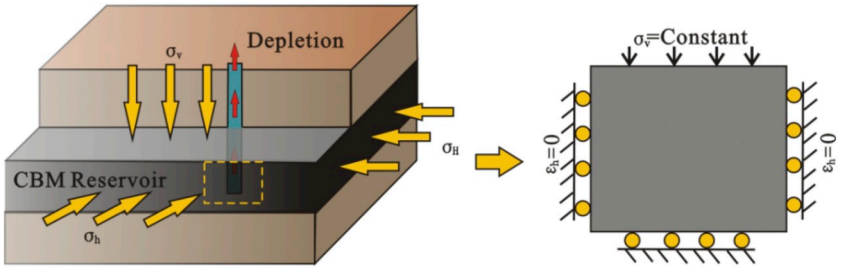

Fig. 9. Sketch of uniaxial strain boundary condition for CBM reservoir.

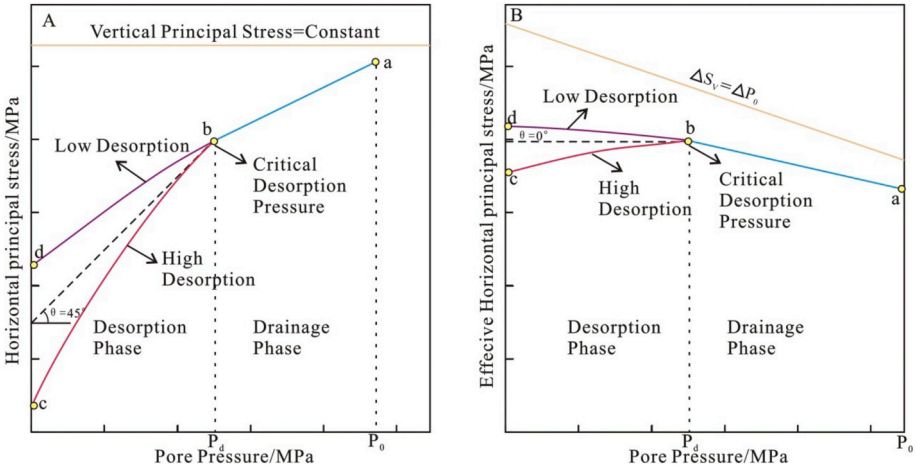

Fig. 10. Change rules of the three principal stress and effective principal stress during the CBM depletion.

5.3.2. Limits of fault friction strength on in-situ stress of ZZ region

Based on the discussion in section 4.2.2, the possible range of in-situ stress magnitudes is limited by the frictional strength of pre-existing faults, which can be used to predict the possible range of in-situ stress magnitudes at a specific depth. According to Eq. (44), the upper bound of S_1 or the lower bound of S_3 can be obtained for different types of faults. The following equation can be acquired:

(1) For a normal fault, the vertical stress (maximum principal stress) can be calculated with Eq. (5). Thus, the lower bound (LB) of the minimum horizontal principal stress (σ_h^{LB}) can be determined as:

$$\sigma_h^{LB} = \frac{\sigma_v - P}{[\sqrt{\mu_i^2 + 1} + \mu_i]^2} + P \tag{48}$$

(2) For a strike-slip fault, the minimum horizontal principal stress (minimum principal stress) can be obtained via hydraulic fracturing.

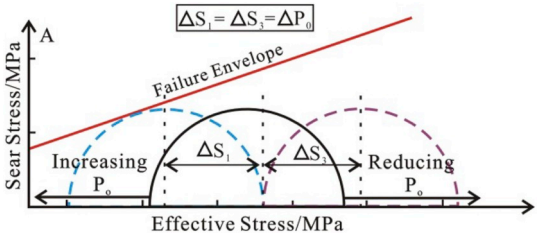

Fig. 11. Mohr circle diagrams illustrating the state of effective stress evolution (the in-situ stresses are assumed to be constant).

The upper bound (UP) of the maximum horizontal principal stress (σ_H^{UB}) can be determined as:

$$\sigma_H^{UB} = [\sqrt{\mu_i^2 + 1} + \mu_i]^2(\sigma_h - P) + P \quad (49)$$

(3) For a reverse fault, the upper bound (UP) of the maximum horizontal principal stress (σ_H^{UB}) can be determined from the vertical stress, as shown in following equation:

$$\sigma_H^{UB} = [\sqrt{\mu_i^2 + 1} + \mu_i]^2(\sigma_V - P) + P \quad (50)$$

Meng et al. (2018) summarized the friction coefficient for different structural planes in sedimentary rock masses, which suggested a friction

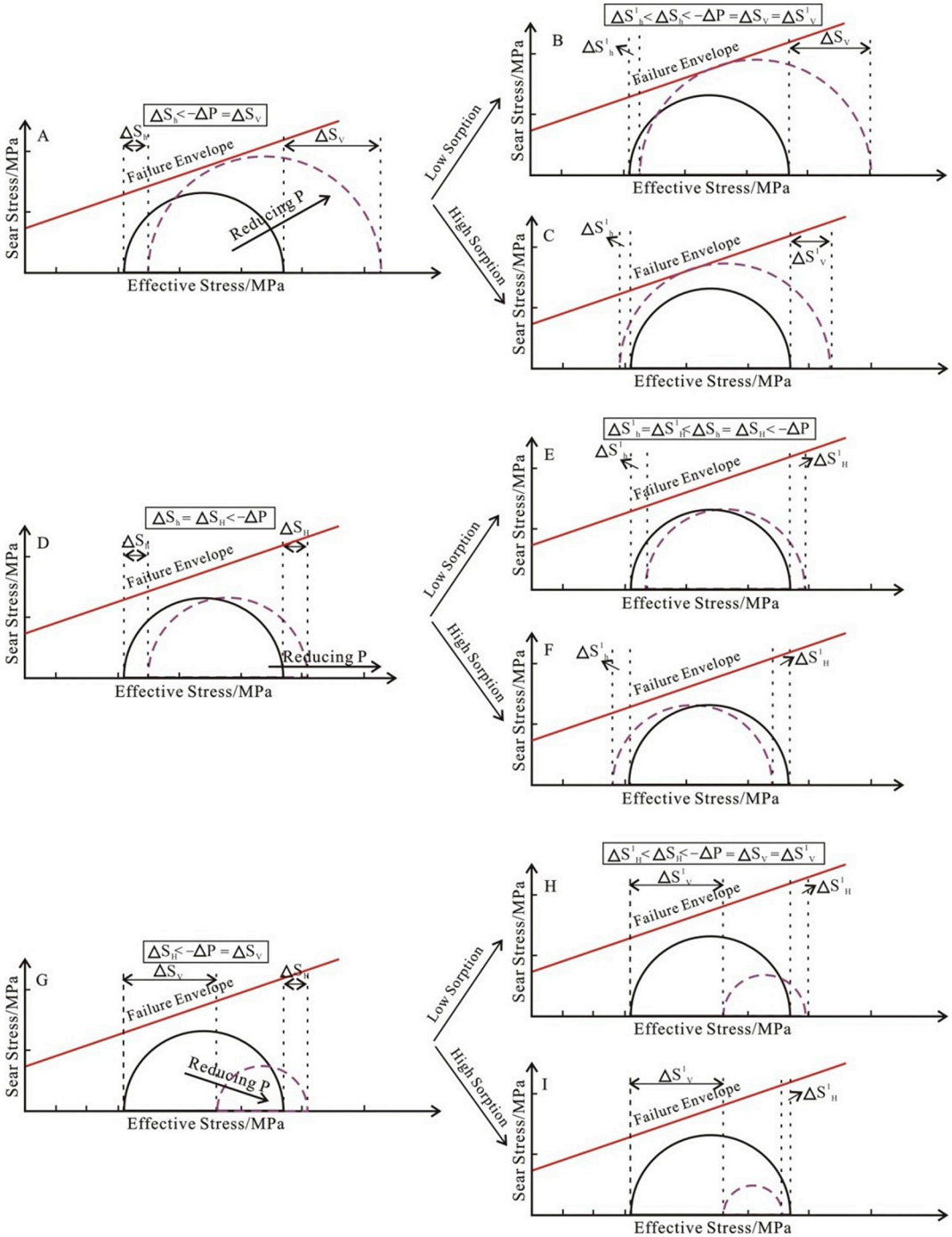

Fig. 12. Mohr circle diagrams illustrating the state of stress evolution with pressure depletion under the uniaxial strain boundary condition;($\sigma_{V0} > \sigma_{H0} > \sigma_{h0}$: A - drainage process, B - Low sorption effect, C - High sorption effect; $\sigma_{H0} > \sigma_{V0} > \sigma_{h0}$: D - drainage process, *E* - Low sorption effect, F - High sorption effect; $\sigma_{H0} > \sigma_{h0} > \sigma_{V0}$: G - drainage process, H - Low sorption effect, I - High sorption effect).

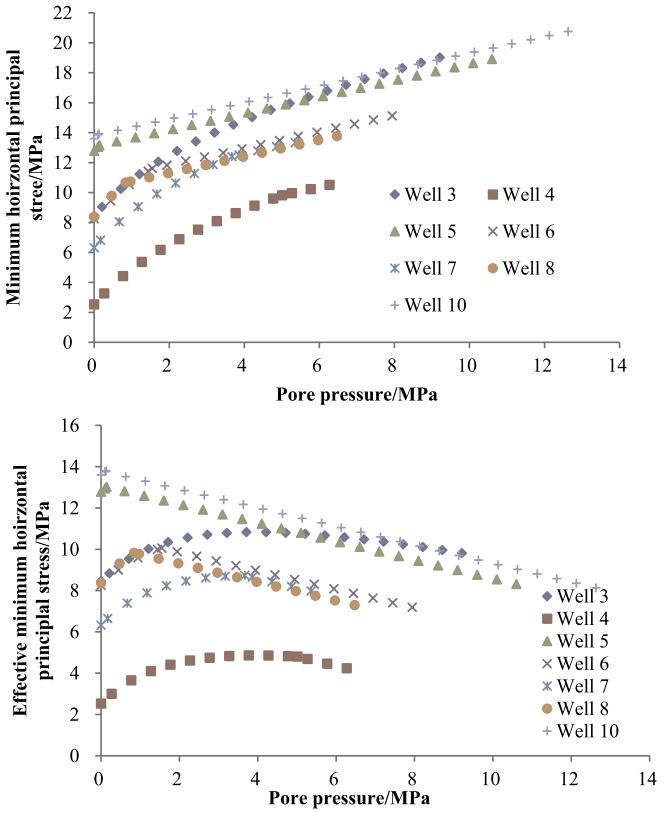

Fig. 13. Change rules of the minimum horizontal principle stress and effective minimum horizontal principle stress during depletion in the normal faulting regime in the ZZ region.

coefficient of approximately 0.6. For the ZZ region, normal faults and strike-slip faults are most common. Thus, the lower bound of the minimum horizontal principal stress within normal stress regimes and the upper bound of the maximum horizontal principal stress within strike-slip normal stress regimes can therefore be calculated for each well, as shown in Fig. 8. In addition, the relationship between the calculated values and the burial depth in the different regime stress states can be expressed as follows:

$$\sigma_h^{LB} = 0.011D + 3.1137 \text{ (Normal faults)} \quad (51)$$

$$\sigma_H^{UB} = 0.055D - 3.2715 \text{ (Strike} - \text{slip faults)} \quad (52)$$

5.3.3. Stability of coal reservoir during depletion in ZZ region

As many normal faults and strike-slip faults are distributed in the ZZ block, the criterion for the failure of normal faulting and strike-slip faulting regimes should be obeyed during depletion. Based on the failure criterion (Eq. (45)), the stability of the CBM reservoirs of the ZZ region during depletion was evaluated under ideal conditions (Table 2). The results indicate that damage is not triggered either in the normal fault regime or in the strike-slip fault regime during drainage. However, damage may occur in the reservoir near some wells during gas desorption. When the pore pressure drops to the critical values (P_{cv}) (1.10 MPa, well 3; 2.57 MPa, well 4; 0.92 MPa, well 6; and 0.28 MPa, well 7), the normal faults near these wells (well 3, 4, 6 and 7) will reactivate. Thus, in order to avoid the formation of coal fines due to reservoir failure, these CBM wells should be kept at a low depletion speed and the bottom hole pressure of these wells should avoid reaching critical pore pressure. This contributes to maintaining the reservoir in a stable state and also causes a large-scale depressurization which can enhance the production of CBM. When the pore pressure is lower than the critical pressure, the speed of depletion should be

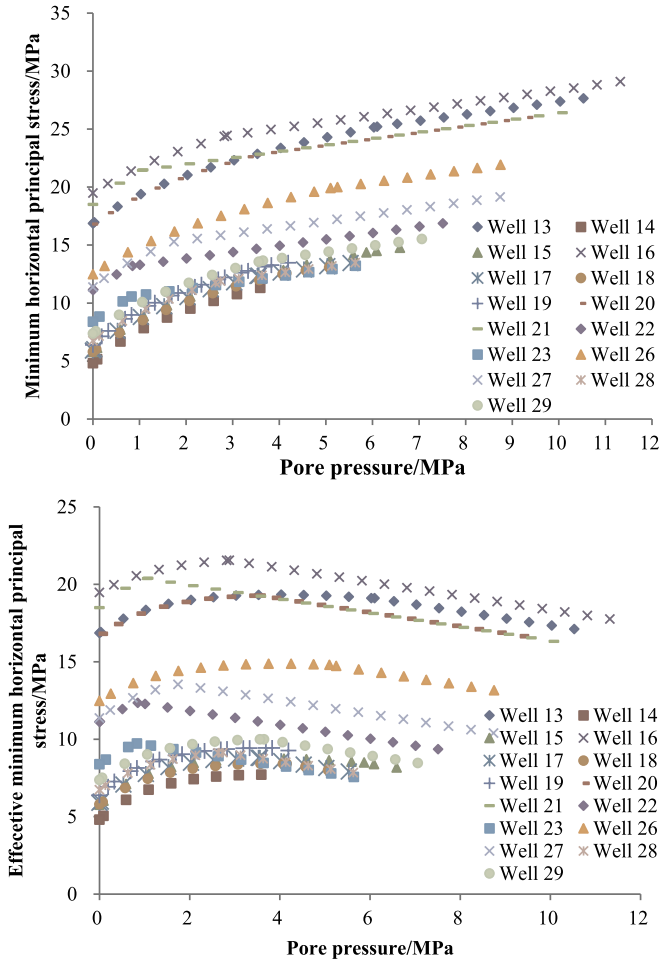

Fig. 14. Change rules of minimum horizontal principle stress and effective minimum horizontal principle stress during depletion in strike-slip faulting regimes of ZZ region.

increased because doing so can prevent the deposition of coal fines in the permeability channels.

6. Conclusion

(1) The ZZ(Zhengzhuang) region is subjected to strong and moderate stress. The fracturing pressure (P_f), closure pressure (P_c), maximum horizontal principal stress (σ_H), and minimum horizontal principal stress (σ_h) correlate positively with the coal buried depth. Although the correlation is not very good, it can also be used to calculate the magnitude of in-situ stress in this region.

(2) The theoretical models describing the response of stress to Coalbed methane (CBM) depletion under uniaxial strain were built, demonstrating the fact that the dynamic evolution of in-situ stress with pore pressure drawdown is a complex process. During drainage, the horizontal principal stress ($\sigma_{H/h}$) decreases and effective horizontal principal stress ($S_{H/h}$) increases linearly with the reduction in pore pressure, but the variation rates of these two parameters are lower than that of the pore pressure. However, during desorption, the law is different. Under low desorption, $\sigma_{H/h}$ decreases and $S_{H/h}$ increases non-linearly with the drop in pore pressure, but the rate of decrease in the low desorption phase is higher than that in the drainage phase and is lower than that of the pore pressure, and the rate of increase is lower than that in the drainage phase. However, under strong desorption, although a non-linear decline of $\sigma_{H/h}$ can be observed, the rate of decline is greater than that of the pore pressure. Meanwhile, there is an

obvious change in $S_{H/h}$, which decrease non-linearly with depletion.

(3) Considering the redistribution of in-situ stress during depletion, criteria for the stress-based failure of CBM reservoirs are suggested. Differences are apparent in the criterion for the failure of a reservoir under different in-situ stress and coal sorption conditions. In a normal faulting stress regime, a reservoir is most easy to be damaged during both drainage and gas desorption; in a strike-slip faulting stress regime, reservoir failure can only be induced during strong desorption; in a reverse faulting stress regime, reservoir failure is not apparent during depletion.

(4) If many faults are developed in a reservoir, the stability of the reservoir is also controlled by the frictional strengths. Fault slipping will occur when the ratio of maximum and minimum principal stress exceeds a value of $[\sqrt{\mu_i^2 + 1} + \mu_i]^2$($\mu_i$ is the friction coefficient). This was applied to calculate the limitation values of the principal stresses of the ZZ region.

(5) The mechanisms governing changes in the in-situ stress and reservoir stability in the ZZ region were also analyzed. Results indicate that the minimum horizontal principal stress (σ_h) decreases and effective minimum horizontal principal stress (S_h) increases linearly with the pore pressure reduction during drainage, which damages the permeability of a CBM reservoir. However, upon entering desorption, σ_h and S_h decrease non-linearly with the drop in pore pressure. The rates of the decrease of σ_h and S_h rise with the increase in gas desorption, which improves permeability. It was also demonstrated that the damage is not triggered in CBM reservoir during drainage. However, on entering gas desorption, when the pore pressure drops to the critical values (1.10 MPa in well 3; 2.57 MPa in well 4; 0.92 MPa in well 6; and 0.28 MPa in well 7), the normal faults near these wells will reactivate, which may produce coal fines and ultimately damage the reservoir permeability.

Declaration of Competing Interest

We wish to confirm that there are no known conflicts of interest associated with this publication and there has been no significant financial support for this work that could have influenced its outcome.

Acknowledgement

This work is financially supported by the Shanxi Province Science and Technology Major Project (Grants 20191102001 and 20181101013), the National Science and Technology Major Project of the Ministry of Science and Technology of China During “13th Five-Year Plan” (Grants 2016ZX05067001-006).

References

Anderson, E.M., 1951. The Dynamics of Faulting and Dyke Formation with Applications to Britain. Hafner Pub. Co.

Bear, J., Corapcioglu, M.Y., 1981. A mathematical model for consolidation in a thermoelastic aquifer due to hot water injection or pumping. Water Resour. Res. 17 (3), 723–736.

Bell, J.S., 1996. Petro geoscience 2. in situ stresses in sedimentary rocks (part 2): applications of stress measurements. Geosci. Can. 23 (3), 135–153.

Byerlee, J., 1978. Friction of rocks. In: Rock Friction and Earthquake Prediction. Birkhäuser, Basel, pp. 615–626.

Cai, Y., Liu, D., Yao, Y., Li, J., Qiu, Y., 2011. Geological controls on prediction of coalbed methane of no. 3 coal seam in Southern Qinshui Basin, North China. Int. J. Coal Geol. 88 (2–3), 101–112.

Chen, S., Tang, D., Tao, S., Xu, H., Li, S., Zhao, J., Li, Z., 2018a. Characteristics of in-situ stress distribution and its significance on the coalbed methane (CBM) development in Fanzhuang-Zhengzhuang Region, Southern Qinshui Basin, China. J. Pet. Sci. Eng. 161 (2018), 108–120.

Chen, S., Tang, D., Tao, S., Xu, H., Zhao, J., Fu, H., 2018b. In-situ stress, stress-dependent permeability, pore pressure and gas-bearing system in multiple coal seams in the Panguan area, western Guizhou, China. J. Nat. Gas Sci. Eng. 49, 110–122.

Dave, A., 2017. Variation of Young’s Modulus with Depletion in Coalbed Methane Reservoirs.

Durucan, S., Edwards, J.S., 1986. The effects of stress and fracturing on permeability of coal. Min. Sci. Technol. 3 (3), 205–216.

Enever, J.R., Henning, A., 1997. The relationship between permeability and effective stress for Australian coal and its implications with respect to coalbed methane exploration and eservoir modelling. In: Proceedings of the 1997 International Coalbed Methane Symposium. 1997. pp. 13–22.

Fan, L., Liu, S., 2018. Numerical prediction of in situ horizontal stress evolution in coalbed methane reservoirs by considering both poroelastic and sorption induced strain effects. Int. J. Rock Mech. Min. Sci. 104 (August 2017), 156–164.

Feng, Q., Wu, C.F., Lei, B., 2011. Coal /rock mechanics features of Qinshui Basin and fracturing crack control. Coal Sci. Technol. 39 (3), 100–103 (in Chinese).

Feng, R., Harpalani, S., Saurabh, S., 2018. Experimental investigation of in situ stress relaxation on deformation behavior and permeability variation of coalbed methane reservoirs during primary depletion. J. Nat. Gas Sci. Eng. 53, 1–11.

Goulty, N.R., 2003. Reservoir stress path during depletion of Norwegian chalk oilfields. Pet. Geosci. 9 (3), 233–241.

Haimson, B.C., Cornet, F.H., 2003. ISRM suggested methods for rock stress estimation—part 3: hydraulic fracturing (HF) and/or hydraulic testing of pre-existing fractures (HTPF). Int. J. Rock Mech. Min. Sci. 40 (7–8), 1011–1020.

Heidbach, O., Rajabi, M., Reiter, K., Ziegler, M., Team, W.S.M., 2016. World Stress Map Database Release 2016. V. 1.1. GFZ Data Serviceshttps://doi.org/10.5880/WSM.2016.001.

Hillis, R., 2000. Pore pressure/stress coupling and its implications for seismicity. Explor. Geophys. 31 (2), 448–454. https://doi.org/10.1071/EG00448.

Hoek, E., Brown, E.T., 1980. Underground Excavations in Rock. Institution of Mining Metallurgy, London, London.

Huang, S., Liu, D., Cai, Y., Gan, Q., 2019. In situ stress distribution and its impact on CBM reservoir properties in the Zhengzhuang area, southern Qinshui Basin, North China. J. Nat. Gas Sci. Eng. 61, 83–96.

Hubbert, M.K., Willis, D.G., 1957. Mechanics of hydraulic fracturing. Petroleum transactions, the American institute of mining. Metal., Petrol. Eng 210, 153–168.

Ju, W., Yang, Z., Qin, Y., Yi, T., Zhang, Z., 2018. Characteristics of in-situ stress state and prediction of the permeability in the Upper Permian coalbed methane reservoir, western Guizhou region, SW China. J. Pet. Sci. Eng. 165, 199–211.

Kang, H., Zhang, X., Si, L., 2009. Study on in-situ stress distribution law in deep underground coal mining areas. In: ISRM International Symposium on Rock Mechanics-SINOROCK 2009. International Society for Rock Mechanics and Rock Engineering.

Kang, H., Zhang, X., Si, L., Wu, Y., Gao, F., 2010. In-situ stress measurements and stress distribution characteristics in underground coal mines in China. Eng. Geol. 116 (3–4), 333–345.

Kim, S., Hosseini, S.A., 2017. Study on the ratio of pore-pressure/stress changes during fluid injection and its implications for CO2 geologic storage. J. Pet. Sci. Eng. 149, 138–150.

Lau, H.C., Li, H., Huang, S., 2017. Challenges and opportunities of coalbed methane development in China. Ener. Fuels 31 (5), 4588–4602.

Laubach, S.E., Marrett, R.A., Olson, I.E., Scott, A.R., 1998. Characteristics and origins of coal cleat: A review. Int. J. Coal Geol. 35 (1–4), 175–207.

Levine, J.R., 1996. Model study of the influence of matrix shrinkage on absolute permeability of coal bed reservoirs. Geol. Soc. Lond., Spec. Publ. 109 (1), 197–212.

Li, Y., Tang, D.Z., Meng, S.Z., Wu, P., 2017. The in-situ stress of coal reservoirs in east margin of Ordos Basin and its influence on coalbed methane development. J. Mining Sci. Technol. 2 (5), 416–424.

Li, G.Q., Yan, D.T., Zhuang, X.G., Zhang, Z., Fu, H.J., 2019. Implications of the pore pressure and in situ stress for the coalbed methane exploration in the southern Junggar Basin. Eng. Geol. https://doi.org/10.1016/j.enggeo.2019.105305.

Liu, S., Harpalani, S., 2013. Permeability prediction of coalbed methane reservoirs during primary depletion. Int. J. Coal Geol. 113, 1–10.

Liu, S., Harpalani, S., 2014. Evaluation of in situ stress changes with gas depletion of coalbed methane reservoirs. J. Geophys. Res. Solid Earth 119 (8), 6263–6276.

Liu, R., Liu, J., Zhu, W., Hao, F., Xie, Y., Wang, Z., Wang, L., 2016. In situ stress analysis in the Yinggehai Basin, northwestern South China Sea: Implication for the pore pressure-stress coupling process. Mar. Pet. Geol. 77, 341–352.

Lv, Y., Tang, D., Xu, H., Luo, H., 2012. Production characteristics and the key factors in high-rank coalbed methane fields: Acase study on the Fanzhuang Block, Southern Qinshui Basin, China. International Journal of Coal Geology 96–97, 93–108. https://doi.org/10.1016/j.coal.2012.03.009.

Matthews, W.R., Kelly, J., 1967. How to predict formation pressure and fracture gradient. Oil Gas J. February, 92–106.

McKee, C.R., Bumb, A.C., Koenig, R.A., 1988. Stress dependent permeability and porosity of coal and other geologic formations. SPE Form. Eval. 3, 81–91.

Meng, Y., 2018. Mechanism of Gas Diffusion-Seepage in High-Rank Coal and Productivity Evaluation of Coalbed Methane Wells. China University of Geosciences Doctoral degree.

Meng, Z., Zhang, J., Wang, R., 2011. In-situ stress, pore pressure and stress-dependent permeability in the Southern Qinshui Basin. Int. J. Rock Mech. Min. Sci. 48 (1), 122–131.

Meng, Z.P., Wang, B.Y., Xie, X.T., Xue, Y.D., Du, X.Y., 2012. Mechanical properties of coal deformation and its influence on permeability. J. China Coal Soc. 37 (8), 1342–1347 (in Chinese).

Meng, Y., Wang, J.Y., Li, Z., Zhang, J., 2018. An improved productivity model in coal reservoir and its application during coalbed methane production. J. Nat. Gas Sci. Eng. 49, 342–351.

Mortazavi, A., Atapour, H., 2018. An experimental study of stress changes induced by reservoir depletion under true triaxial stress loading conditions. J. Pet. Sci. Eng. 171, 1366–1377. https://doi.org/10.1016/j.petrol.2018.08.047.

Nowacki, W., 1975. Dynamic Problems of Thermoelasticity. Springer Science & Business Media.

Palmer, I., Mansoori, J., 1998. How permeability depends on stress and pore pressure in

coalbeds: A new model. In: SPE annual technical conference and exhibition, held in Denver, 6–9 October.
Pan, Z., Connell, L.D., 2012. Modelling permeability for coal reservoirs: A review of analytical models and testing data. Int. J. Coal Geol. 92, 1–44.
Paul, S., Chatterjee, R., 2011. Determination of in-situ stress direction from cleat orientation mapping for coal bed methane exploration in south-eastern part of Jharia coalfield, India. Int. J. Coal Geol. 87 (2), 87–96.
Rajabi, M., Heidbach, O., Tingay, M., Reiter, K., 2017. Prediction of the present-day stress field in the Australian continental crust using 3D geomechanical–numerical models. Aust. J. Earth Sci. 64 (4), 435–454.
Saurabh, S., Harpalani, S., 2018. Stress path with depletion in coalbed methane reservoirs and stress-based permeability modeling. Int. J. Coal Geol. 185 (November 2017), 12–22.
Segall, P., Fitzgerald, S.D., 1998. A note on induced stress changes in hydrocarbon and geotherma. Tectonophysics 289, 117–128.
Shen, J., Qin, Y., Li, Y., Yang, Y., Ju, W., Yang, C., Wang, G., 2018. In situ stress field in the FZ Block of Qinshui Basin,China: Implications forthe permeability and coalbed methane production. Journal of Petroleum Science and Engineering 170, 744–754. https://doi.org/10.1016/j.petrol.2018.07.011.
Shi, J.Q., Durucan, S., 2004. Drawdown induced changes in permeability of coalbeds: a new interpretation of the reservoir response to primary recovery. Transp. Porous Media 56 (1), 1–16.
Shi, J.Q., Durucan, S., 2005. A model for changes in coalbed permeability during primary and enhanced methane recovery. SPE Reserv. Eval. Eng. 8 (4), 291–299.
Townend, J., Zoback, M.D., 2000. How faulting keeps the crust strong. Geology 28 (5), 399–402.
Wang, M., Zhu, Y.M., Li, W., Zhong, H.Q., Wang, Y.H., 2012. Tectonic evolution and reservoir formation of coalbed methane in Zhengzhuang region of Qinshui basin. J. China Univ. Ming Technol. 41 (3), 425–431.
Wang, X.X., Liu, X., Xie, W., Zheng, X.T., Jia, Y.G., 2016. Analysis of gas control activity on coalbed methane caused by strike-slip structures in Qinshui basin. Coal Technol. 35 (7), 110–112 (in Chinese).
Xie, S.R., Yang, B., Zhang, Q., Song, H.Z., Suo, H.X., Zhang, T., 2019. Research on lift pressure system with combined pipeline and intensive drill-hole gas drainage along the layer in low permeability coal seam. J. Mining Sci. Technol. 4 (1), 34–40.
Zhang, C., Chen, Q., Qin, X., Hong, B., Meng, W., Zhang, Q., 2017. In-situ stress and fracture characterization of a candidate repository for spent nuclear fuel in Gansu, northwestern China. Eng. Geol. 231, 218–229.
Zhao, Y.S., Hu, Y.Q., Wei, J.P., Yang, D., 2003. The experimental approach to effective stress law of coal mass by effect of methane. Transp. Porous Media 53 (3), 235–244.
Zhao, J., Tang, D., Lin, W., Qin, Y., Xu, H., 2019. In-situ stress distribution and its influence on the coal reservoir permeability in the Hancheng area, eastern margin of the Ordos Basin, China. J. Nat. Gas Sci. Eng. 61 (June 2018), 119–132.
Zoback, M.D., 2010. Reservoir Geomechanics. Cambridge University Press.
Zoback, M.D., Healy, J.H., 1984. Friction, faulting, and “in situ” stresses. Ann. Geophys. 2, 689–698.
Zoback, M.D., Barton, C.A., Brudy, M., Castillo, D.A., Finkbeiner, T., Grollimund, B.R., Moos, D.B., Peska, P., Ward, C.D., Wiprut, D.J., 2003. Determination of stress orientation and magnitude in deep wells. Int. J. Rock Mech. Min. Sci. 40 (7–8), 1049–1076.